INL/CON-12-25760
PREPRINT

Particle Image Velocimetry Measurements in a Representative Gas-Cooled Prismatic Reactor Core Model: Flow in the Coolant Channels and Interstitial Bypass Gaps

IMECE2012

Thomas E. Conder
Richard S. Skifton
Ralph S. Budwig

November 2012

The INL is a
U.S. Department of Energy
National Laboratory
operated by
Battelle Energy Alliance

Proceedings of the ASME 2012 International Mechanical Engineering Congress & Exposition
IMECE2012
November 9-15, 2012, Houston, Texas, USA

IMECE2012-87549

PARTICLE IMAGE VELOCIMETRY MEASUREMENTS IN A REPRESENTATIVE GAS-COOLED PRISMATIC REACTOR CORE MODEL: FLOW IN THE COOLANT CHANNELS AND INTERSTITIAL BYPASS GAPS

Thomas E. Conder
Idaho National Laboratory
Idaho Falls, ID 83415

Richard S. Skifton
University of Idaho
Idaho Falls, ID 83415

Ralph S. Budwig
University of Idaho
Boise, ID, 83702

ABSTRACT

Core bypass flow is one of the key issues with the prismatic Gas Turbine-Modular Helium Reactor, and it refers to the coolant that navigates through the interstitial passages between the graphite fuel blocks instead of traveling through the designated coolant channels. To determine the bypass flow, a double scale representative model was manufactured and installed in the Matched Index-of-Refraction flow facility at Idaho National Laboratory; after which, stereo Particle Image Velocimetry (PIV) was employed to measure the flow field within. PIV images were analyzed to produce vector maps, and flow rates were calculated by numerically integrating the velocity field. It was found that the bypass flow varied between 6.9-15.8% for channel Reynolds numbers of 1,746 and 4,618 with a 6mm gap. The results were compared to computational fluid dynamic (CFD) pre-test simulations. When compared to these pretest calculations, the CFD analysis appeared to under predict the flow through the gap.

BYPASS FLOW PROBLEM

Bypass flow is a unique characteristic to the Gas Turbine-Modular Helium Reactor (GT-MHR) design. For a prismatic type, core it refers to the coolant that navigates through the interstitial passages between the fuel elements and reflector regions in lieu of traveling through the designated coolant channels. It is estimated that bypass flow will vary from 10-25% or more of the total core flow and it may also vary over time due to fast neutron-induced graphite element shrinkage and core barrel swelling [1]. These flows are of particular concern because they reduce the desired flow rates in the coolant channels, and thereby may have significant influence on the maximum fuel element temperature, cooling channel exit temperature, and the temperature distribution in the lower plenum; all which affect the efficiency of the reactor. Bypass flow is considered the most important contributor to uncertainty in fuel temperatures [2].

PRISMATIC FUEL BLOCK DESIGN

The GT-MHR by General Atomics is designed with a prismatic type core and uses helium as its coolant [3]. This type of core consists of a large group of tightly stacked hexagonal graphite prismatic fuel elements. The blocks are arranged in the reactor vessel with inner and outer graphite reflector regions that surround an annular core of fuel blocks (See Fig. 1).

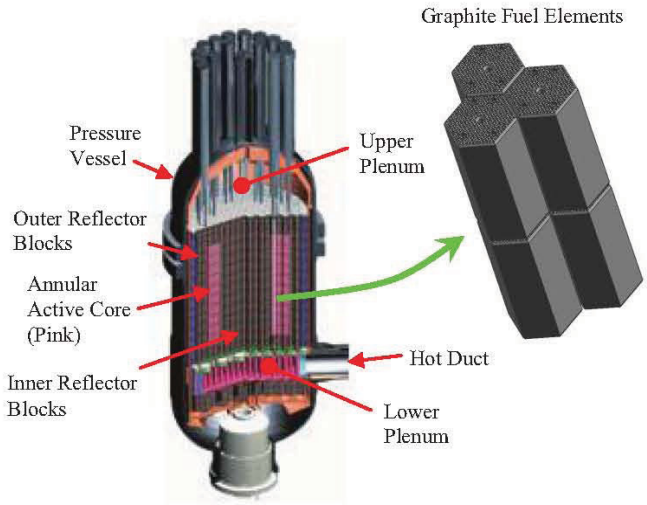

Figure 1. Gas Turbine-Modular Helium Reactor Schematic

During operation, cold Helium flows from the outer annulus of the hot duct, up the walls of the pressure vessel, and into the upper plenum. The coolant then travels downward through a series of stacked graphite fuel blocks which contain an array of coolant channels. The mass flow rate for the helium is expected to reach 320 kg/s at full power. During normal operation, the coolant channel outlet Reynolds number varies from approximately 57,000 at high power to 2,300 at ten percent core power. Table 1 contains select specifications for the GT-MHR.

Table 1. Selected GT-MHR Design Parameters [3]

Specification	Value
Core Power (MW)	600
Helium Mass Flow Rate (kg/s)	320
Active Core Pressure Drop (MPa)	0.051

FUEL ELEMENT GEOMETRY

Active core fuel elements are manufactured from H-451 graphite in the form of right hexagonal prisms. Each element measures 793mm high and 360mm across its flats (See Fig. 2). An array of fuel holes and coolant channels, with diameters of 12.7 and 15.88mm, respectively, run parallel through the length of each prism in a regular, triangular pattern. At the center of each block is a fuel handling hole, surrounded by six small coolant channels with diameters of 12.7mm.

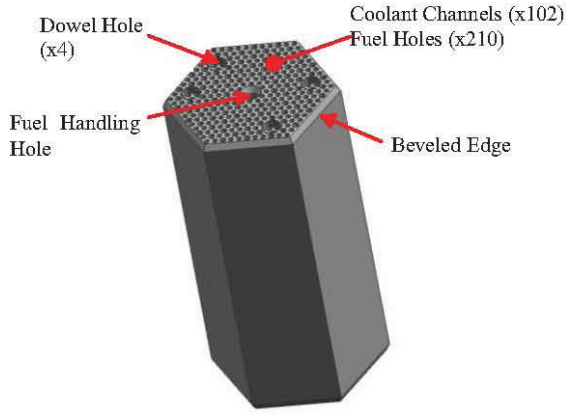

Figure 2. Standard Fuel Element

The blocks are aligned primarily using a dowel-socket connection with its upper and lower neighbors, and are designed to closely fit together. The top and bottom edges of each element are beveled, with dimensions of 17.145mm and 8.304mm. The bevel is used to assist insertion of the elements into the core. Table 2 contains a list of pertinent fuel element parameters for the present study.

The gaps between fuel elements have a maximum width of approximately 3.9mm upon installation. Though the fuel elements are designed to tightly pack the core, it is known that they will change size over their lifetime [4].

Table 2. Pertinent Fuel Element Parameters [3]

Parameter	Value
Distance Across Flats (m)	0.36
Element Height (m)	0.7930
Coolant Holes per Element, Small/Large	6/102
Coolant Hole Diameter, Small/Large (mm)	12.7/15.88
Fuel Holes per Element	210
Fuel Hole Diameter (mm)	12.7
Control Rod Hole Diameter (mm)	101.6
Triangular Pitch Between Coolant Holes (mm)	18.796
Beveled Edge, Height/Width (mm)	17.145/8.304

Graphite expands as temperature increases and is expected to shrink slightly due to irradiation. Melese et al. estimates a decrease of 5.1mm in height and 3.5mm across the flats over a four year lifespan. Since neither temperature nor irradiation is uniform, these effects will modify the shape of the elements and unevenly influence the gap size between adjacent blocks. The spacing between each block will vary depending on such graphite shrinkage, manufacturing tolerances, and inexact installation. These gaps between the fuel elements allow for the helium coolant to travel in two general flow paths: axially—parallel to the coolant channels and radially—in between the stacked fuel blocks.

BYPASS FLOW LITERATURE REVIEW

Several studies in the 1980's presented one-dimensional nodal and analytical methods to investigate bypass flow [5, 6]; however, these methods were quite simplistic. In recent years, studies have focused on Computational Fluid Dynamic (CFD) calculations performed by researchers from Idaho National Laboratory (INL), Japan Atomic Energy Research Institute, and the Korea Atomic Energy Research Institute. Presently, there are limited experimental studies that focus on bypass flow. Thus, accurate fluid dynamic experiments must be performed to validate CFD based research and predictions.

Sato et al. performed three-dimensional CFD calculations of a typical 600 megawatt Very High Temperature Reactor (VHTR) core [7]. Their model represented a one-twelfth sector of a hexagonal fuel block, which was selected to achieve the smallest possible symmetric slice. The simulation considered an inlet temperature of 490°C, a mass flow rate of 0.2 kg/s, and a heat generation rate of 27.88 MW/m^3 with uniform gaps. The region between the fuel blocks was varied for each simulation using 0, 3, and 5mm spacing. This variation in gap width caused the channel Reynolds number to range between 20,000 and 35,000 for the largest and smallest gap, respectively. The results indicated that the gap to coolant channel flow fraction increased from 4.15-9.78% considering a gap width increase from 3 to 5mm. Also, with increasing gap size: the maximum fuel temperature increased by 62°C, the temperature difference variation between coolant channels increased by 101°C, and the maximum channel outlet temperature decreased by 55°C. These changes established a large lateral thermal gradient across the

sector and increased the possibility of hot streaking in the lower plenum.

Yoon et al. studied the bypass flow of a prismatic modular reactor (PMR) design using both experimental and computational methods [8]. For their model, they introduced the concept of a unit-cell, which included 3 sectors, each made from a one-sixth part of a prismatic fuel block, and was separated by a uniform gap. The coolant channels for each sector were represented by a single 0.12m tube, equivalent to the total flow area. The total unit-cell area made up one-half a prismatic fuel block. The gaps were varied by 3 and 5mm. Using air at 25°C, the inlet flow rate was varied to achieve approximately 0.18, 0.37, and 0.56 kg/s, with estimated channel Reynolds numbers ranging from 32,000-99,000. Using these inlet conditions, it was found that the bypass ratio varied from 2.48-5.70% for the 3mm gap and 7.52-11.97% for the 5mm gap. Fluid dynamic computations were performed for the 5mm case using the SST turbulence model with 2.9 million elements; however, differences as high as 27% were calculated from the experimental results. Other model combinations for bypass flow around a reflector block were studied; however, those cases were not considered here.

Pre-test CFD calculations for the present Bypass Flow Experiment were carried out by Johnson at the INL [9]. The geometry was nearly identical to the present study, with the exception that symmetry was applied and a one-sixth sector was selected; the model was composed of 1.5 coolant channels and half a gap width. The coolant path consisted of an upper plenum, a full-length fuel element, and then a partial-length fuel element. This geometry allowed for both axial and radial gaps. The axial gaps varied in size by 2, 6, and 10mm and the radial gaps varied by 2 and 10mm. Mineral oil was selected as the working fluid at 25°C and volumetric flow rates of 205.3 and 57.2 L/min were used. The k-ε turbulence model was employed with near wall treatment, and the solution was iterated to residuals less than 1×10^{-4}. Table 3 contains a summary of the results.

Upon observation of the table, it is understood that:

- The bypass flow fraction in the upper block was higher than the lower block for all cases.
- Flow in the gap increased with increasing gap size.
- The bypass flow fraction in the 6mm axial gap was similar for both the low and high flow rate cases, even though one was laminar and one was turbulent.
- Flow in the channels was turbulent in all cases.
- Flow in the gap was laminar in all cases, except the high flow rate, 10mm axial gap scenario.

Table 3. Summary of CFD Calculations for One-sixth Sector of the Bypass Model (results taken from Johnson, 2010)

Axial Gap (mm)	2		6			10
Radial Gap (mm)	2	10	2	10	2	2
Flow Rate (L/min)	205.3	205.3	205.3	205.3	578.2	578.2
$Re_{Channel}$	6,387	6,387	5,440	5,400	15,024	12,362
Re_{Gap}	31	32	524	543	1,668	3,192
Pressure Drop (kPa)	13.5	13.7	10.4	10.6	64.7	45.3
Bypass Flow Upper Block (%)	0.97	0.97	15.6	16.2	17.3	31.9
Bypass Flow Lower Block (%)	0.61	0.65	13.4	12.4	14.9	29.9

BYPASS FLOW EXPERIMENT

An experimental study at INL investigated the behavior of flow in the interstitial regions between fuel blocks of a VHTR design—in particular the goal was to quantify the flow through the gap in relation to the coolant channels. This study was carried out in the Matched Index of Refraction Flow Facility (MIR) and Particle Image Velocimetry (PIV) was used to measure the flow field within a scaled model. A simplified model of the GT-MHR was considered, wherein a stacked junction of six adjacent fuel blocks were represented. Fuel block geometry was scaled by a factor of 2.016 to geometrically match the prismatic core configuration. Figure 3 illustrates the cross-section of the bypass model and the vertex of three adjoining fuel blocks from which it was derived. As shown, a small gap existed between the blocks, depicting the interstitial gap region. The cross-section of the model consisted of three sectors of intersecting prismatic fuel blocks, and included 9 coolant channels and 3 axial gaps. Additionally, each fuel block was carefully sectioned to only include the area that reasonably influenced the flow into the coolant channels and interstitial gaps.

The scaling factor was selected based on the commercially available diameter quartz tubes—used as the coolant channels for the model—that would permit Reynolds numbers comparable to the low power range of an operational prismatic reactor. In addition, careful selection of the scaling factor was important as it was the key feature to provide adequate spatial resolution for stereo PIV measurements in the coolant channels and gap. Based on this criterion, a tube diameter of 32mm was chosen.

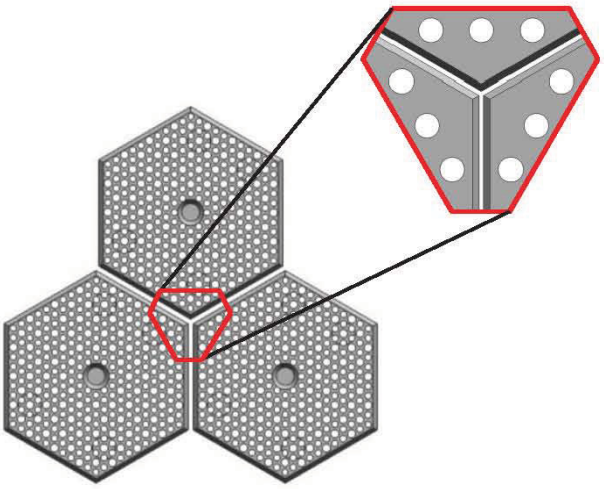

Figure 3. Bypass Model Relationship to GT-MHR

The experimental apparatus included two near double scale blocks: a full-length upper block and a 20% partial-length lower block. Each sector was manufactured from three parallel tubes that connected to a solid, machined cap on each end. The caps were chamfered to match those of a typical fuel block. Long plates extended between the caps to serve as walls for the interstitial gaps. All quartz components were manufactured to a 0.127mm tolerance. The gaps between sectors were adjustable to approximately 2, 6, and 10mm widths using a spacer that runs along the length of the model. Epoxy adhesive and RTV silicone were used to bond and seal the model; however, optical glue was used to seal the joints where optical or laser access was required.

The model was constructed from fused quartz to permit optical access for PIV measurements. Quartz was used because its refractive index is similar to mineral oil, the working fluid in the MIR facility. By pairing these media at their index matching temperature—25.156°C, the model became near invisible when submersed in the mineral oil, and optical refraction was eliminated between the wall of the test section and the inside of the model. This technique is advantageous to measure internal flow.

Figure 4 depicts the components of the bypass flow model. Flow entered the model through the inlet annulus, where it was directed to the periphery of a hemisphere. The hemisphere contained an anti-separation spike which prohibited the flow from separating as it turned 180° to travel through the upper plenum, and representative fuel blocks.

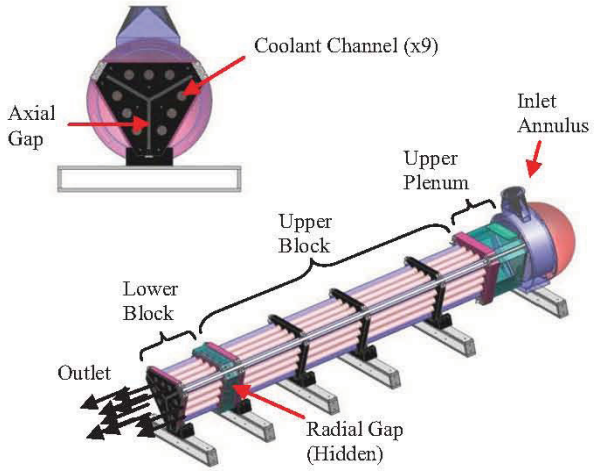

Figure 4. Bypass Model Components

A pump analysis of the total dynamic head for the bypass flow model was performed to estimate the Reynolds numbers expected in the coolant channels and gaps given the MIR system; specifically, an auxiliary loop pump—provided flow into the model, MIR plumbing, and bypass model geometry. Figure 5a illustrates the auxiliary loop pump curve and estimated head loss with varying flow rate. Figure 5b shows expected Reynolds numbers in the coolant channels and gaps for varying flow rates. It was determined that a maximum flow rate of 1430 L/min could be achieved given a 6mm gap width—leading to channel and gap Reynolds numbers of 7,282 and 360, respectively. This maximum assumes little or no leakage from the model.

The gap width was used as the characteristic length to calculate the Reynolds number in the gap, which allowed direct comparison to the CFD pre-calculations performed by Johnson.

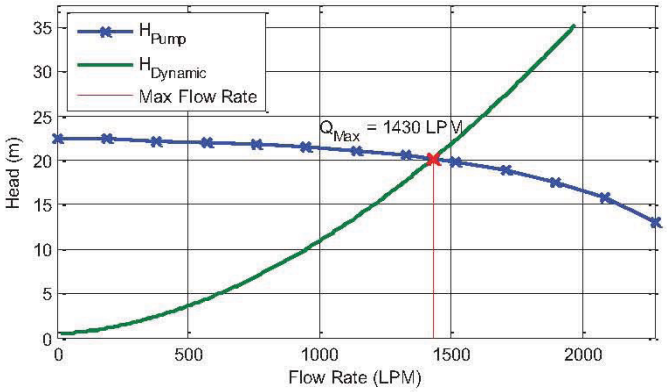

Figure 5a. Head Loss Calculations

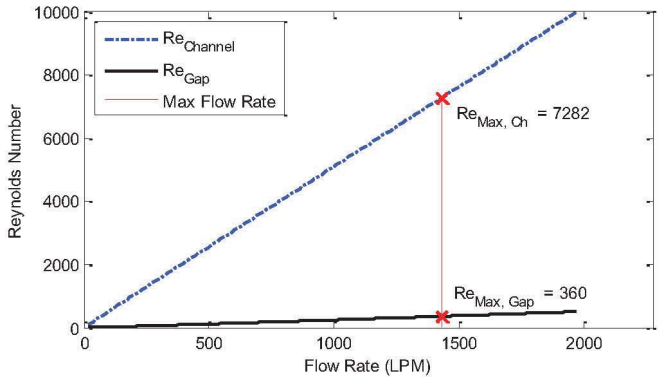

Figure 5b. Design Head Loss and Reynolds Number Estimates

Because the MIR is an isothermal facility, the effects of density gradients and the influence of temperature will not be studied. The present experiment will focus on the flow regimes that are momentum-dominated as opposed to density-gradient dominated.

TEST PLAN

Stereo PIV was used to capture the flow field within the upper plenum, coolant channels, and gaps. The flow was seeded with 12μm diameter silver coated hollow glass spheres, which illuminated in 532nm laser light. An Nd:YAG double pulsed laser projected a light sheet upward through the bottom of the model in the stream-wise direction and two special CCD cameras continuously imaged the seeding particle movement. Sequential images were broken down into interrogation windows and statistical algorithms were employed to determine particle movement, after which, velocity vectors were calculated over the field of view (FOV). A sample size of 500 vector maps was used to ensemble average each flow field measurement.

Measurements were taken in three stream-wise locations: in the upper plenum and in the midsection of both the upper and lower fuel blocks (See Fig. 6). In these locations, the laser light sheet and cameras were translated across the width of the model, and velocity fields were measured at millimeter intervals—301, 245, and 245 slices were taken in the upper plenum, upper block, and lower block, respectively. As a note, the model's origin was located at the centerline of the model and the inlet of the upper plenum.

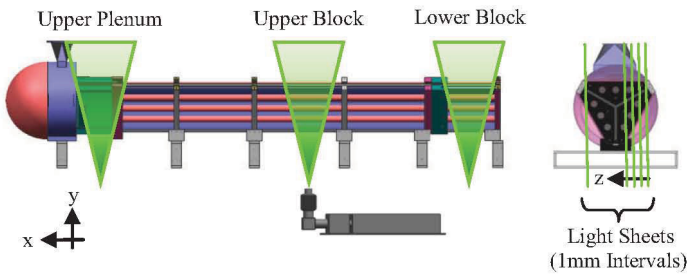

Figure 6. Light Sheet Locations

Table 4 contains the data collection matrix for the present experiment. Inlet conditions were varied to incorporate laminar, transitional, and turbulent flows in the coolant channels. For the contents of this paper, the axial and radial gaps were held constant using nominal values of 6 and 2mm, respectively.

Table 4. Bypass Flow Experiment Test Matrix

			Light Sheet Positions in 1 mm Intervals		
Re_{Ch}	Axial Gap (mm)	Radial Gap (mm)	Upper Plenum (mm)	Upper Block (mm)	Lower Block (mm)
1700	6.05	2.02	-152 < z < +152	-122 < z < +122	-122 < z < +122
2800	6.05	2.02	-152 < z < +152	-122 < z < +122	-122 < z < +122
4500	6.05	2.02	-152 < z < +152	-122 < z < +122	-122 < z < +122

During model assembly, spacers were used to achieve uniform axial gaps; however, after installation in the test section the interstitial gap width was measured and found to vary between 5.47-7.75mm. Figure 7 illustrates the actual widths of the interstitial gap for the cross-section of the bypass model measured at the inlet of the upper block. The assembled gap had a cross-sectional area that was approximately 0.0028m^2.

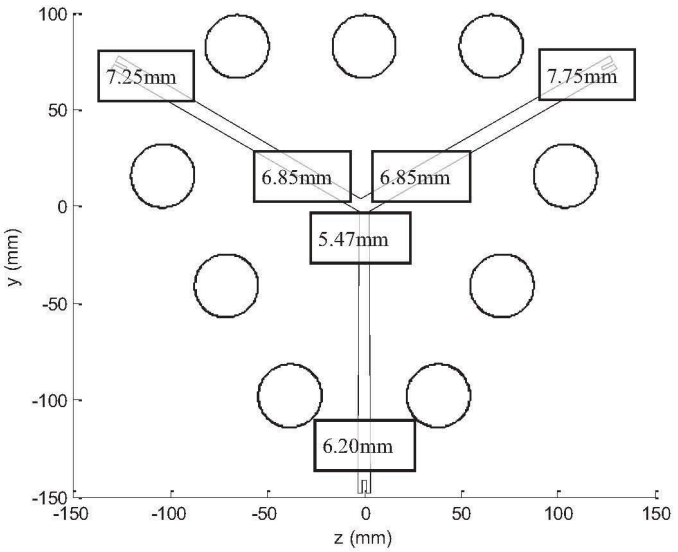

Figure 7. Actual Gap Spacing about the Model Cross-Section

EXPERIMENTAL METHODS

The model was installed and aligned in the MIR test section within 0.076mm of being level, plumb, and square to the traversing system—the apparatus used to position the cameras.

The main loop circulated mineral oil around the model at 0.15m/s to maintain temperature within ±0.005°C of matching temperature. The flow rate into the model was adjusted to approximate the desired Reynolds numbers from the test matrix.

Velocity measurements were realized using commercially available PIV software with twin, double-pulsed 532nm Nd-YAG lasers. Two 1.9 megapixel cameras focused on the model through 50mm lenses at acute angles (less than 15°) to the test section windows. Small angles were desired to minimize refraction at the test section air-to-window interface. Scheimpflug adapters were installed to give a sharp focus over the entire FOV.

The cameras were calibrated using a split level 309x309mm plate that filled the entire FOV. The plate was manufactured with an array of 3mm dots that were 15mm apart, and 3mm between levels. A polynomial model was applied to map the FOV, after which, self-calibration was performed to correct any misalignment of the laser light sheet. The light sheet was adjusted to a thickness of 1mm which allowed for complete coverage of the model within the limits of the test matrix.

An interrogation window of 12x12 pixels was chosen for processing, and flow was seeded such that at least 8-10 particle pairs were in each window. The cameras collected data at a frame rate of 15Hz. The time delay between sequential frames was chosen based on the criteria set by Wilson and Smith [10]—particle displacements were limited to traveling between 25-62.5% of the interrogation window.

Images were processed first with a 16x16 interrogation window size and then with a 12x12, using 50% overlap for both. The interrogation window was selected such that the smallest feature size, the gap, had a minimum of 4-5 vectors after processing.

A GPU based PC, with 580 cores, processed the data using the direct cross-correlation method. Due to storage and processing requirements, each span-wise velocity measurement was stored on a single 2 terabyte removable hard drive. The prescribed test matrix produced about 18 terabytes of data, taking over 3 months to process.

PIV SAMPLE SIZE ANALYSIS

An analysis similar to Uzol and Camci [11] helped estimate the sample size "N" (i.e. number of vectors maps) that needed to be averaged to calculate stable vector and turbulence quantities which were independent of time. The analysis was conducted using 4000 instantaneous vector maps for a typical slice of the flow at a 600L/min flow rate ($Re_{Ch} \approx 2800$).

At a specific location in the FOV, sets of "N" instantaneous vectors were randomly selected (from the available 4000), averaged, and plotted in relation to the total mean. This process was repeated 100 times for each "N" to statistically depict how the spread in the average decreased with increasing sample size. "N" was varied between 5 and 4000 samples. It was noted that in calculating the ensemble-average for the flow field, some regions of the FOV converged slower than others (i.e. required more images). Hence, the slow convergent regions dictated the number of images required to calculate an accurate ensemble-average. The above mentioned process was completed over an entire FOV (containing channel and gap flow) to determine the location of slowest convergence. Figure 8 illustrates the convergence at a typical point in the flow for mean velocity and turbulent variation with increasing sample size. It was determined that 500 samples could adequately represent velocity and turbulence quantities given the space requirement and computational cost of the test matrix.

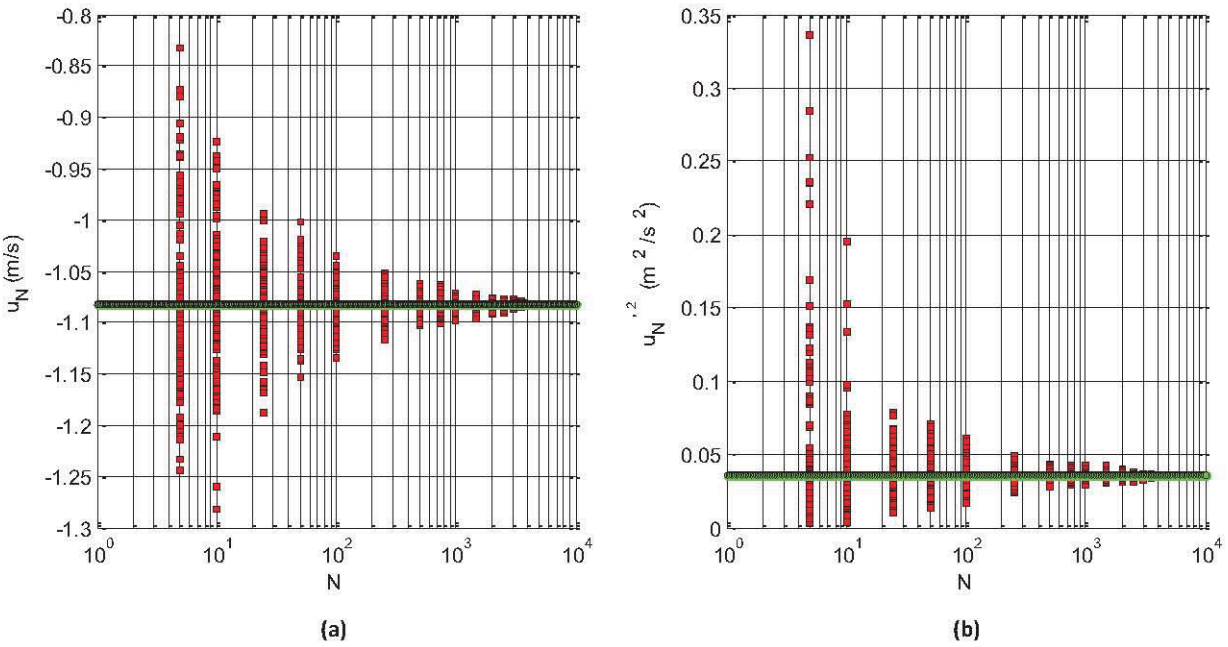

Figure 8. Variation in (a) Mean Velocity and (b) Mean Turbulence Stress versus Sample Size

FLOW RATE ANALYSIS

To quantify the flow of the gap in relation to the coolant channels, velocities from the cross-section of the model were needed. To this end, time averaged vector maps at each stream-wise location and flow rate were compiled into matrices, after which, data slices were taken at three locations perpendicular to the flow at x = -113.1mm, -1029.5mm, -1928.5mm (See Fig. 9). For the purpose of this paper, the measurements taken in the upper plenum were used solely as a flow rate check.

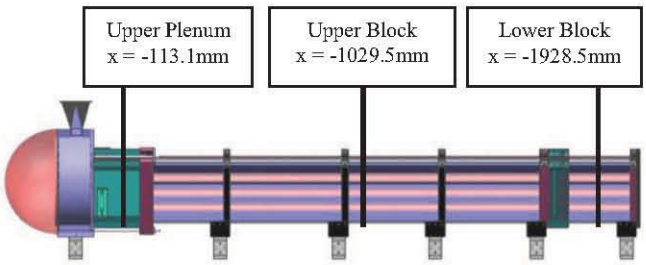

Figure 9. Data Slice Locations

A typical slice of the bypass data located in the upper and lower blocks is displayed in Figure 10. This plot denotes the velocity contours through the cross-section of the model. Note: The PIV cameras had limited optical access to the upper three coolant channels. As such, the PIV algorithms did not detect movement of particles and effectively calculated streaks of zero velocity in these locations.

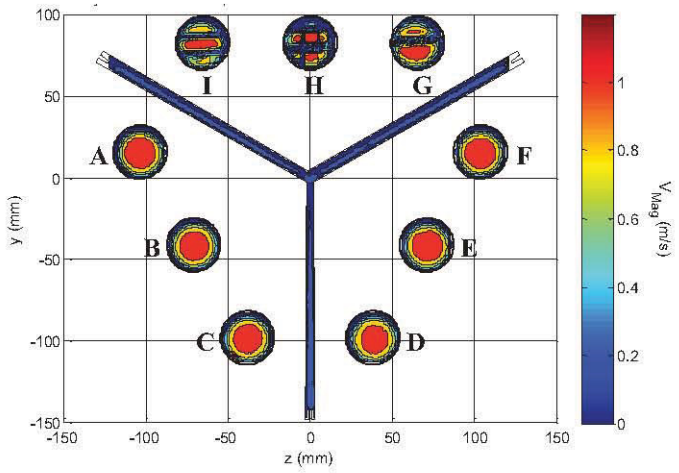

Figure 10. Typical Velocity Contour Plot (Q = 351.15 L/Min and x = -1029.5mm)

The commercial software MATLAB was used to compile the vector maps because of its ability to manipulate large matrices. A geometric mask was applied to the data to disregard vectors outside the flow area. The remaining zones were subdivided into small rectangular regions, sized by the light sheet spacing (dz) and interrogation window height (dy); the area of which was defined by $dA = dz \cdot dy$. Figure 11 illustrates the typical method for discretizing the flow area to calculate a flow rate within a coolant channel. Flow in the gaps and upper plenum were calculated in a similar fashion.

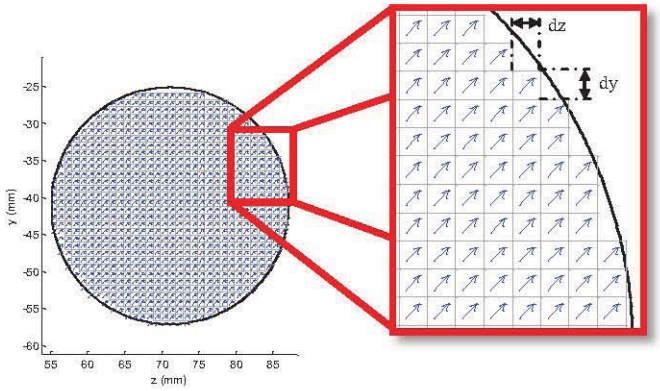

Figure 11. Typical Flow Area Discretization of a Coolant Channel. (Note: represented vectors are for illustrative purposes and do not accurately represent the flow along the axis of the tube.)

The flow rate was calculated by multiplying each vector by dA and summing over the masked flow field. The following equation described the method to calculate the flow rate (Q).

$$Q \cong \sum_{i=0}^{N} \sum_{j=0}^{M} V_{(i,j)} \cdot dA$$

To determine the accuracy of PIV for the purpose of calculating the bypass ratio, the results were compared to flow rate measurements taken near the inlet of the model using a calibrated turbine flow meter (TFM), accurate to within ±0.05% of the reading.

RESULTS AND DISCUSSION

The distribution of flow through the lower six channels and the axial gap is presented in Table 5. As expected, the calculated flow rates through the channels were similar for a given inlet condition. It was noted that with an increase in flow rate, the flow through the gap increased and the variation in flow rate between the coolant channels increased.

Table 5. Flow Distribution within the Bypass Model

		Flow Rate (L/Min)						
TFM Reading (L/Min)	Stream-wise Location (mm)	A	B	C	D	E	F	Gap
351.1	-1029.5	34.8	34.4	34.7	34.0	35.7	35.5	28.8
579.9		57.6	56.5	57.1	54.0	57.2	57.2	69.5
1004.1		91.0	89.3	90.6	88.1	91.1	91.9	152.7
351.1	-1928.5	35.4	34.6	34.7	35.5	36.6	37.4	24.1
579.9		55.3	55.7	54.9	55.2	56.9	57.5	55.9
1004.1		90.9	90.4	91.4	91.8	94.1	96.0	142.3

Using the flow rates presented in Table 5, approximate channel Reynolds numbers of 1750, 2800, and 4550 were calculated. Development lengths were predicted for these flows from equations summarized by Munson et al. [12]. It was estimated that fully developed flow would occur near 3.4, 3.0, and 0.6m for the 351.1, 579.9, and 1004.1 L/Min flow rate cases, respectfully. As the model length is 1.91m, it was understood that only the highest flow case would be fully developed within the coolant channels. Figure 12 shows the typical variation in time averaged velocity for a flow within a coolant channel. As expected, the lower Reynolds number cases show a developing velocity profile.

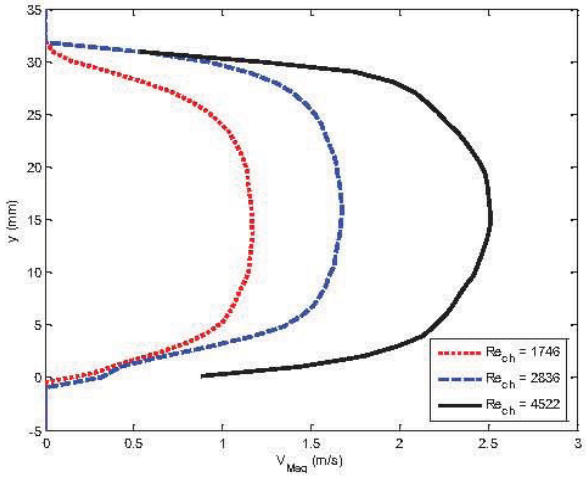

Figure 12. Typical Variation of Time Averaged Velocity in a Coolant Channel located at [x, z] = [-1,029.5, 103]mm

Figure 13 illustrates the time averaged velocity through an axial gap located at [x, z] = [-1029.5, 0]. As shown, the flow located at the vertex (i.e. y = 0) had the highest velocity within the axial gap. Johnson also observed this flow characteristic in his preliminary calculations, noting that this region was of lower

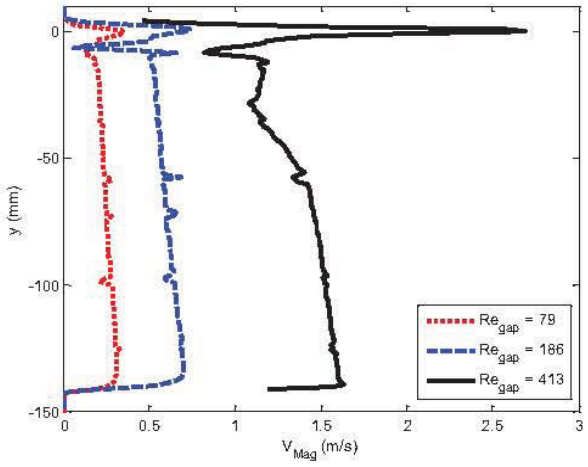

Figure 13. Variation of Time Averaged Velocity in a Gap located at [x, z] = [-1029.5, 0]mm

flow resistance. Just below the vertex, the velocity gradually increased toward the perimeter of the model. Recalling the gap was not uniform and the width of the gap increased from 5.47-6.2mm between the vertex and the perimeter of the model, it was understood that higher velocities occurred where the gap was largest.

Flow rate calculations were computed for each case in the test matrix. It was observed that calculated flow rate error varied between 6.2-10.5% when compared to the TFM reading. For the lowest and highest flow rates, the bypass flow ratio ranged from 7.3-16.94%. Due to lack of optical access in the upper three tubes of the model, it was assumed these velocity quantities were inaccurate. For this reason, the average velocity of all six lower coolant channels was superimposed on the upper channels to estimate a more realistic flow rate. Figure 14 illustrates the superposition principle using data from Figure 10. In this case, the average flow of channels A, B, C, D, E, and F was superimposed on the upper three channels G, H, and I.

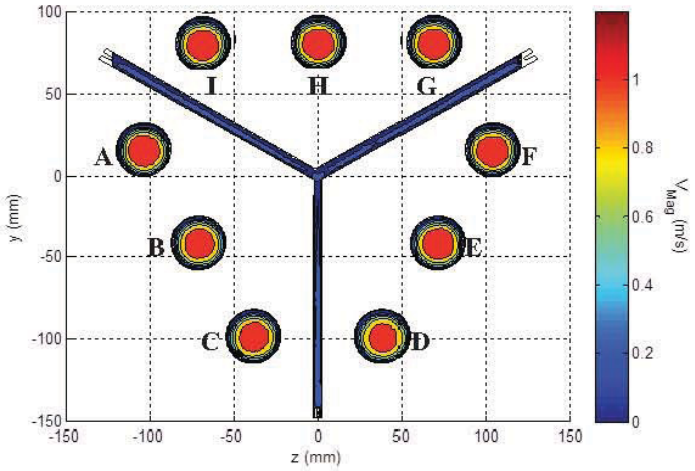

Figure 14. Superimposed Velocity Contour Plot (Q = 351.15 L/Min and x = -1029.49mm)

Table 6 contains flow rate calculations, errors, and bypass flow ratios considering the superimposed data. As expected, the calculated flow rate error decreased substantially. However, manipulating the data had little effect on the bypass flow ratio.

Table 6. Bypass Flow Results for a Scaled 3mm Gap Width (Superimposed Data on Upper 3 Tubes)

TFM Reading (L/Min)	Stream-wise Location (mm)	PIV Calculated Flow Rate (L/Min)	Calculated Flow Rate Error (%)	Re_{Ch}	Re_{Gap}	Bypass Flow (%)
351.1	-1029.5	342.50	2.46	1746	79	8.40
579.9		579.01	0.015	2836	186	12.00
1004.1		965.55	3.84	4522	413	15.82
351.1	-1928.5	345.46	1.62	1789	66	6.96
579.9		558.94	3.61	2778	150	9.99
1004.1		974.14	2.98	4618	382	14.61

Through observation, it was seen that the bypass flow in the upper block was higher than that of the lower block for all flow rates within the test matrix. Accordingly, it was understood that the flow redistributes via the radial gap, entraining oil into the coolant channels and starving the gap in the lower block.

In relating the present study to the CFD calculations, it was noted that the flow rates considered by Johnson were considerably higher than those achieved in the present study. For this reason, only the high flow experimental case was effectively compared (i.e. $Re_{Ch} \approx 4550$). A graph of the experimental and CFD bypass flow ratio results versus channel Reynolds number is shown in Figure 15. For the flow rate of 1231.8 L/min, CFD estimated the channel and gap Reynolds numbers as 5440 and 524. As expected, the present study showed that the lower flow rate of 1004 L/min produced Reynolds numbers of 4512 and 412 for the coolant channel and gap, respectively. However, in examining the bypass ratio for both cases, it appears that the CFD under predicts the amount of flow traveling through the gaps in both the upper and lower blocks.

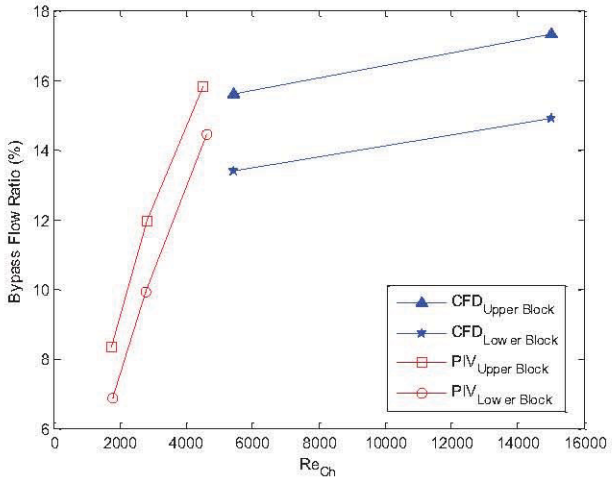

Figure 15. Comparison of CFD and Experimental Data

CONCLUSION

Velocity measurements were taken in the INL MIR facility to measure the anticipated bypass flow associated with a prismatic Gas Turbine-Modular Helium Reactor. A model which represented a stacked junction of six partial fuel blocks with nine coolant tubes and axial and radial gaps was manufactured and installed in the MIR; after which, stereo PIV was employed to measure the flow field within. Measurements were taken in three locations along the length of the model: in the upper plenum and in the midsection of both the large and small fuel blocks. Flow rates were calculated for the coolant channels and gaps for comparison. The bypass ratio was estimated to range from 6.8-15.8% for the considered flow rates. When compared to pretest calculations, the CFD analysis appeared to under predict the flow through the gap.

ACKNOWLEDGEMENTS

This project was supported by the DOE VHTR program at Idaho National Laboratory. The authors are grateful to Dr. Hugh McIlroy who was instrumental in the development of the model concept and test plan. The authors would like to thank Robert Pink, Russ Lewis, Neil Boyce, Richard Hatch, Ryan Davis, and Paul Nardone for their assistance with the experiment fabrication, assembly, and installation.

REFERENCES

[1] INEEL, 2005, "Next Generation Nuclear Plant Research and Development Program Plan", *INEEL/EXT-05-02581*.

[2] INL, 2010, "Next Generation Nuclear Plant Methods Technical Program Plan", *INL/EXT-06-11804*.

[3] General Atomics, 1996, "Gas Turbine-Modular Helium Reactor (GT-MHR) Conceptual Design Description Report", Doc. 910, 720 Rev1.

[4] Melese, G., Katz, R., 1984, "Thermal and Flow Design of Helium-Cooled Reactors", *American Nuclear Society*, La Grange Par, IL.

[5] Kaburaki, H., Takizuka, T., 1987, "Effect of Crossflow on Flow Distribution in HTGR Core Column", *J. of Nuclear Sci. and Tech*, **24**, pp. 516-525.

[6] Suzuki, K., Suzuki, K. Mogi, H., Fumizawa, M., Iyoku, T, Sawa, K., 1985, "Analysis of Core Flow Deviation Caused by the Large Gaps Between Horizontal Block Interfaces", Specialists meeting on Safety and Accident Analysis for Gas-Cooled Reactors, Oak Ridge, TN.

[7] Sato, H., Johnson, R., and Schutz, R., 2010, "Computational Fluid Dynamic Analysis of Core Bypass Flow Phenomena in a Prismatic VHTR", *Annals of Nuclear Energy*, **37**, pp. 1172-1185.

[8] Yoon, S., Cho, Y., Kim, K., Kim, M., Lee, W., and Park, G., 2007, "Experimental Evaluation of the Bypass Flow in the VHTR Core," *SMiRT-19*, Toronto.

[9] Johnson, R., 2011, "Pre-Test CFD Calculations for a Bypass Flow Standard Problem", *ASME IMECE*, Denver, CO.

[10] Wilson, B., Smith, B., 2011, "Errors in Mean and Fluctuating Velocity Due to PIV Bias and Precision Uncertainties", *NURETH-14*, Toronto, Canada.

[11] Uzol, O., Camci C., 2001, "The Effect of Sample Size, Turbulence Intensity and the Velocity Field on the Experimental Accuracy of Ensemble Averaged PIV Measurements", *Proc. of 4th Int. Sym. on Particle Image Velocimetry*, Gottingen, Germany.

[12] Munson, B., Young, D., Okiishi, T., 2004, *A Brief Introduction to Fluid Mechanics*, Wiley, Ed. 3, pp. 312.